J Low Temp Phys (2011) 162: 354–360
DOI 10.1007/s10909-010-0266-4

Turbulent Superfluid Profiles in a Counterflow Channel

L. Galantucci · C.F. Barenghi · M. Sciacca · M. Quadrio · P. Luchini

Received: 15 June 2010 / Accepted: 26 October 2010 / Published online: 6 November 2010

Abstract We have developed a two-dimensional model of quantised vortices in helium II moving under the influence of applied normal fluid and superfluid in a counterflow channel. We predict superfluid and vortex-line density profiles which could be experimentally tested using recently developed visualization techniques.

Keywords Superfluid helium · Turbulence · Vortices

L. Galantucci (✉) · M. Quadrio
Dipartimento di Ingegneria Aerospaziale, Politecnico di Milano, via La Masa, 34, 20156 Milano, Italy
e-mail: galantucci@aero.polimi.it

M. Quadrio
e-mail: maurizio.quadrio@polimi.it

Present address:
L. Galantucci · M. Sciacca
School of Mathematics and Statistics, Newcastle University, Newcastle upon Tyne NE1 7RU, UK

C.F. Barenghi
School of Mathematics and Statistics, Newcastle University, Newcastle upon Tyne NE1 7RU, UK
e-mail: c.f.barenghi@ncl.ac.uk

M. Sciacca
Dipartimento di Metodi e Modelli Matematici, Università di Palermo, Viale delle Scienze, 90128 Palermo, Italy
e-mail: msciacca@unipa.it

P. Luchini
Dipartimento di Ingegneria Meccanica, Università di Salerno, via Ponte don Melillo, 84084 Fisciano (Salerno), Italy
e-mail: luchini@unisa.it

1 Motivation

The recent development of visualization techniques in superfluid helium based on micron-size tracers [1, 2] has raised the possibility of experimentally determining superfluid and normal fluid profiles and the spatial distribution of quantised vortices in a channel, thus solving outstanding problems in quantum turbulence. Particularly interesting (and relevant to engineering applications) is the turbulence induced by heat transfer (counterflow turbulence). It is well known that if the applied heat flux $\dot{Q}$ is less than a small critical value $\dot{Q}_c$ then the heat is carried by the normal fluid component, and the superfluid component flows in the opposite direction to conserve mass. If $\dot{Q} > \dot{Q}_c$ the superfluid component becomes turbulent, forming a disorganized tangle of quantised vortices. In some geometries, at larger heat flux a transition to a more intense vortex tangle has been observed [3], which is perhaps related to the onset of turbulence in the normal fluid [4].

In this paper we are concerned with the intermediate heat transfer regime, in which the normal fluid is still laminar, but the superfluid forms a turbulent tangle. The issue which we address is the average superfluid profile and the average spatial distribution of vortices in the channel. Let $\mathbf{v}_n$ and $\mathbf{v}_s$ be respectively the normal fluid and superfluid velocity fields. The normal fluid satisfies no slip boundary conditions at the wall of the channels, so, for the sake of simplicity, we assume that $\mathbf{v}_n$ is a steady classical parabolic Poiseuille profile (corresponding to the analytical laminar solution of the Hall-Vinen-Bekarevich-Khalatnikov (HVBK) equations [5]). This approximation implies that the constant pressure drop along the channel is the same with and without the vortex tangle. The superfluid slips at the boundaries, so, in the absence of vortices, it is natural to assume that $\mathbf{v}_s$ has a constant (uniform) profile. The velocity fields $\mathbf{v}_n$ and $\mathbf{v}_s$ are related by the counterflow condition of no net mass flow along the channel.

The question which we ask is the following: if $\dot{Q} > \dot{Q}_c$, are the vortices uniformly distributed in the channel, or do they organize themselves spatially, creating a non-uniform superfluid profile at scales larger than the average vortex separation ℓ but smaller than the channel size D?

2 Model

To answer the question we consider the following idealised two-dimensional model which, we argue, captures the most important physical ingredients. Let x and y be respectively directions along and across the channel, with walls at $y = \pm D/2$ and periodic boundary conditions at $x = 0$ and $x = \lambda$. The normal fluid velocity is $\mathbf{v}_n = (v_n^x, v_n^y) = (-V_{n0}[1 - (2y/D)^2], 0)$ with $V_{n0} > 0$ and thus pointing in the negative x direction. The superfluid velocity $\mathbf{v}_s = (v_s^x, v_s^y)$ is decomposed in two parts, $\mathbf{v}_s = \mathbf{v}_{s0} + \mathbf{v}_{si}$; the former is the uniform flow $\mathbf{v}_{s0} = V_{s0}(t)\hat{\mathbf{x}}$, $\hat{\mathbf{x}}$ being the unit vector along x, and the latter, $\mathbf{v}_{si}$, is the velocity field induced by N vortex points located at positions $\mathbf{r}_j = (x_j(t), y_j(t))$ (for $j = 1, \ldots, N$) where t is time. Half the vortices have positive circulation $\Gamma_j = \kappa$, and half have negative circulation $\Gamma_j = -\kappa$, where $\kappa = 10^{-3}$ cm^2/s is the quantum of circulation in superfluid ^{4}He. To satisfy the superfluid's boundary condition that $v_s^y = 0$ at $y = \pm D/2$ (no flow into the wall), we

attach to each vortex point an infinite series of image vortex points in the positive and negative regions $y > D/2$ and $y < -D/2$ [6].

The equation of motion of a vortex located at $\mathbf{r}_j$ is [7]

$$\frac{d\mathbf{r}_j}{dt} = \mathbf{v}_s(\mathbf{r}_j) + \alpha \mathbf{s}'(\mathbf{r}_j) \times (\mathbf{v}_n(\mathbf{r}_j) - \mathbf{v}_s(\mathbf{r}_j)) + \alpha'(\mathbf{v}_n(\mathbf{r}_j) - \mathbf{v}_s(\mathbf{r}_j)), \tag{1}$$

where $\mathbf{s}'_j$ is the unit vector along the vortex j (in the positive or negative z direction) and α and α' are temperature dependent mutual friction coefficients [8].

The quantity V_{s0} is determined at each time t by imposing the counterflow condition

$$\rho_n \langle v_n^x \rangle + \rho_s \langle v_s^x \rangle = 0, \tag{2}$$

where ρ_n and ρ_s are the temperature-dependent normal fluid and superfluid densities, $\rho = \rho_n + \rho_s$ is the total helium density, and $\langle v_n^x \rangle$ and $\langle v_s^x \rangle$ are the channel averages of the x-components of the normal fluid and superfluid velocities, defined as

$$\langle v_s^x \rangle = \frac{1}{\lambda D} \int_0^\lambda \int_{-D/2}^{D/2} v_s^x(x, y) dx dy = V_{s0} + \frac{1}{\lambda D} \int_0^\lambda \int_{-D/2}^{D/2} v_{si}^x(x, y) dx dy \tag{3}$$

and

$$\langle v_n^x \rangle = \frac{1}{D} \int_{-D/2}^{D/2} v_n^x(y) dy = -\frac{2}{3} V_{n0}. \tag{4}$$

To model the creation and the destruction of vortices (mechanisms intrinsically 3-dimensional) within our 2-dimensional model, we proceed as follows. When the distance between two vortex points of opposite circulation becomes smaller than a critical value ϵ_1, we perform a "numerical vortex reconnection" and remove these vortex points; similarly, when the distance between a vortex point and a boundary is less than $\epsilon_2 = 0.5\,\epsilon_1$, we remove this vortex point (the vortex of opposite circulation being the nearest image vortex beyond the wall). To maintain a steady state, when a vortex point is removed, a new vortex point of the same circulation is re-inserted into the channel, either on the axis ($y = 0$) or near the walls or randomly, as described in the next section. This reconnection model, corresponding 3-dimensionally to the vortex filament method of Schwarz [7], correctly describes the fate of two very near antiparallel vortices (as confirmed by past Gross-Pitaevskii numerical studies [9]) and avoids the generation of infinitesimal length scales which would trigger numerical instabilities.

At selected times, given the vortex configuration $\mathbf{r}_j(t)$ ($j = 1, \ldots, N$), we define a *coarse-grained* superfluid velocity $\bar{\mathbf{v}}_s$ by averaging the components of the (microscopic) velocity $\mathbf{v}_s$ over channel strips of size Δ in the y direction, such that $\ell < \Delta < D$. The limit $\ell \ll \Delta \ll D$ corresponds to the HVBK equations [10]. We assume that the velocity $\bar{\mathbf{v}}_s$ is parallel to the walls, $\bar{\mathbf{v}}_s = (\bar{v}_s, 0)$. The curl of $\bar{\mathbf{v}}_s$ can be interpreted as the coarse-grained superfluid vorticity.

To make connection with the experiments, we interpret $n = N/(\lambda D)$ (number of vortex points per unit area) as the vortex line density L (vortex length per unit volume), from which $\ell = n^{-1/2}$ is the average intervortex spacing. The imposed heat

flux $\dot{Q}$, which is reported in experiments, is related to the average counterflow velocity $V_{ns} = \langle v_n^x \rangle - \langle v_s^x \rangle$ by the relation $\dot{Q} = T\rho_s S V_{ns}$, where T is the temperature and S the specific entropy.

The calculation consists in computing the evolution of the vortex points, starting from an arbitrary initial condition, until a steady state regime is achieved and the profile of $\bar{\mathbf{v}}_s$ becomes constant. The time integration is performed using the second-order Adams-Bashfort method with time step Δt.

3 Results

The numerical code solves the governing equations written in dimensionless form. The units of length, velocity and time are respectively $\delta_c = D/2 = 4.55 \times 10^{-3}$ cm, $u_c = \kappa/(2\pi\delta_c) = 3.49 \times 10^{-2}$ cm/s, $t_c = \delta_c/u_c = 0.13$ s. Non-dimensional quantities are denoted by the superscript '$*$'. We choose parameters taking into account the available computing power and the experiments of Tough and collaborators [11, 12]: $\lambda^* = 6$, $T = 1.7$ K, $D^* = 2$ (corresponding to tube $R4$ in Ref. [11]), $\epsilon_1 = 1.25 \times 10^{-2}\,\ell$, $\Delta = 1.25\,\ell$ and $\Delta t^* = 1.9 \times 10^{-6}$.

We set the values $N = 1876$ and $V_{ns}^* = -478.5$ according to (34) in [11] in order to reproduce the statistically-steady-state present at $T = 1.7$ K. Using (2), (4) and the definition of V_{ns} we have $V_{n0}^* = 553.6$. The vortex density is $n^* = 156.3$, and the average intervortex spacing, $\ell^* \approx 0.08$, corresponds to the dimensionless number $L^{1/2}D = D^*\sqrt{n^*} = 25$. This value of $L^{1/2}D$ is typical of counterflow experiments [12] and, on the basis of experimental data and discussions reported in past He II counterflow studies [11, 12], is sufficiently high to properly define the continuous mean mesoscopic fields $\bar{\mathbf{v}}_s$ and $\bar{\boldsymbol{\omega}}_s$ but still consistent with the laminar normal fluid flow assumption.

At the temperature $T = 1.7$ K, taking into account pressure and temperature variations experimentally measured along the channels [11], we can assume (*incompressibility approximation*) the constant values $\rho_s = 0.112$ g cm^{-3}, $\rho_n = 3.32 \times 10^{-2}$ g cm^{-3} and $S = 0.395$ J (g K)$^{-1}$ [13].

To distinguish the three different "re-nucleation" regimes, hereafter we indicate with (a) random vortex-reinsertion in the channel, and with (b) and (c) vortex reinsertion on the axis and near the walls, respectively.

Case (a) is the simplest and corresponds physically to 3-dimensional superfluid vorticity production taking place throughout the vortex-tangle due to reconnections and vortex-rings emission. The initial condition, shared by all three cases, is shown in Fig. 1 (left) and consists of a random vortex configuration. During the evolution of case (a), positive and negative vortices move on the average towards the $y^* = +1$ and $y^* = -1$ wall respectively. The trajectory of an individual vortex can be very irregular, due to the interaction with other vortices. A drift in the positive x direction is superimposed to this motion towards walls.

After a time-interval of the order of $\tau_a^* \approx 2 \times 10^{-2}$, the vortex configuration reaches a steady state, as illustrated in Fig. 1 (right). Note that there are more positive vortices in the $y^* > 0$ region and more negative vortices in the $y^* < 0$ region, as confirmed by the density profile of positive vortices, $n_+^*(y^*)$, shown in Fig. 3 (right)

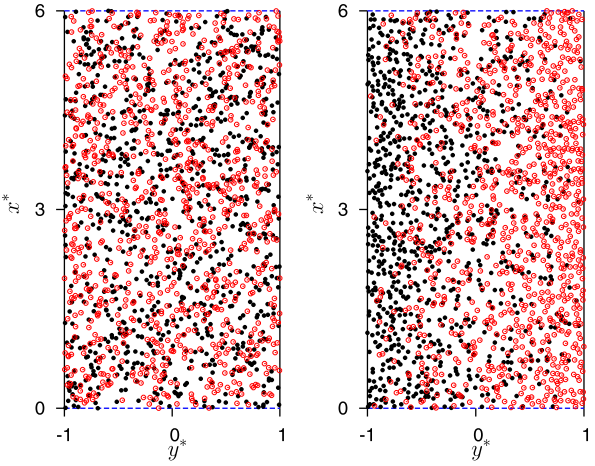

Fig. 1 (Color online) Initial random vortex configuration (*left*) and vortex configuration at $t^* = 4.75 \times 10^{-2}$ (*right*). Positive and negative vortices are respectively denoted by *empty* (*red*) and *filled* (*black*) circles

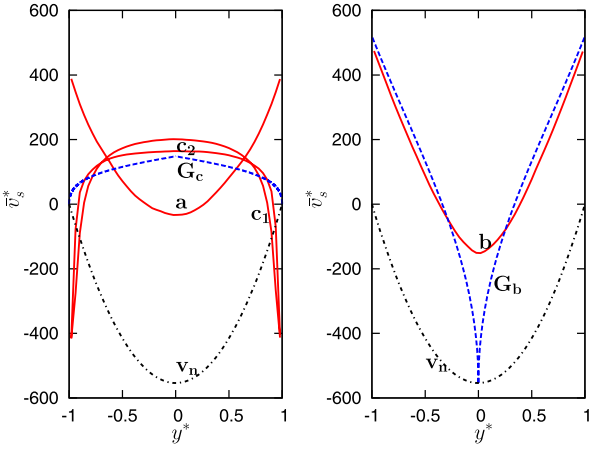

Fig. 2 (Color online) *Solid* (*red*) *line*: coarse-grained superfluid velocity $\bar{v}_s^*(y^*)$; the labels (a), (c_1), (c_2) (*left*) and (b) (*right*) correspond to the cases discussed in the text. *Dashed* (*blue*) *line*: analytical laminar solution [15] of HVBK equations which applies Geurst's approach [5] to Cartesian geometry. Curves G_c (*left*) and G_b (*right*) correspond respectively to cases (c) and (b) in the text. *Dot-dashed* (*black*) *line*: normal fluid velocity profile (*left*, *right*)

(the density profile of negative vortices, $n_-^*(y^*)$, is symmetrical with respect to the channel axis). The polarization of the vortex configuration is not complete—not *all* positive vortices are in $y^* > 0$ and not *all* negative vortices are in $y^* < 0$—in agreement with arguments discussed in Ref. [14].

The resulting coarse-grained superfluid velocity profile associated to this partial polarization is compared to the driving normal fluid velocity in Fig. 2 (left): we find that the profile is almost parabolic, $\bar{v}_s^* \sim y^{*2.19}$. The distribution of vortices irrespective of their sign, $n^*(y^*)$, is almost constant, as shown in Fig. 3 (left).

The other two cases which we investigate, case (b) (nucleation at $y^* = 0$) and case (c) (nucleation at $y^* = \pm 1$), are suggested by the analysis of Geurst [5] based on the HVBK equations. Case (b) induces a vortex density profile $n^*(y^*)$ with a sharp peak near $y^* = 0$ (Fig. 3 (left)). We find that this concentration of vortices on the axis is unstable: collective motion of vortices of the same polarity appears, and the resulting coarse-grained superfluid velocity profile, $\bar{v}_s^*(y^*)$, shown in Fig. 2 (right), undergoes small-amplitude but persistent oscillations. A power-law regression yields

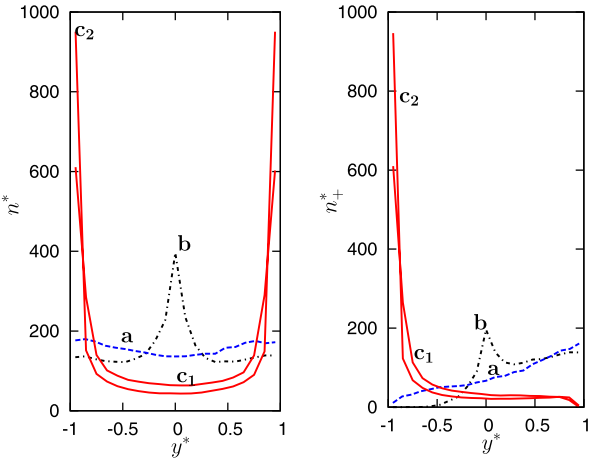

Fig. 3 (Color online) Vortex density $n^*(y^*)$ (*left*) and positive vortex density $n^*_+(y^*)$ (*right*) for cases: (*a*), *dashed* (*blue*) *line*; (*b*), *dot-dashed* (*black*) *line*; (c_1) and (c_2), *solid* (*red*) *lines*

the dependence $\bar{v}_s^* \sim y^{*1.6}$; as in case (a), after a transient of the order of $\tau_b^* \sim 6 \times 10^{-2}$, we obtain the partially polarized steady state vortex–distribution shown in Fig. 3 (right).

Finally, we consider case (c). This nucleation regime corresponds physically to 3-dimensional superfluid vorticity production arising from vortex–rings emission by vortices pinned to the walls. In our model, the positive (negative) vortex points are re-inserted near (rather than at) the $y^* = -1$ ($y^* = +1$) wall, in order not to collapse rapidly on the boundaries due to the Magnus-mutual friction forces balance. Let ξ be the distance of nucleation away from the walls. To investigate the dependence of the flow on ξ, we choose values $\xi_1 = \ell$ and $\xi_2 = 0.5\,\ell$, which we refer to as cases (c_1) and (c_2). The resulting coarse-grained superfluid velocity profile $\bar{v}_s^*(y^*)$ in the two cases is shown in Fig. 2 (left): note the reversed concavity, compared to cases (a), (b) and the normal fluid.

Figure 3 shows that the nucleation location clearly influences the vortex distribution and the steady state vortex density profile $n^*(y^*)$, which is reached after a transient time interval of the order of $\tau_c^* \approx 3 \times 10^{-2}$, independently of ξ.

4 Discussion

The model which we have presented, being 2-dimensional, is clearly rather idealized, and we do not claim that it is possible to make direct comparison with experiments. Nevertheless, the model contains what we argue are the most important physical ingredients, and it allows us to make predictions about the vortex distribution and the superfluid profile across a channel at small values of the applied heat flux. The 2-dimensional solution which we have found can be interpreted in 3-dimensions as vortex loops which move from the outer parts of the channel towards the centre, speeding up during this process, or, perhaps more precisely, as a tangle which is polarised by the presence of such loops.

Our coarsed-grained superfluid velocity profile $\bar{v}_s^*(y^*)$ compares very well with the 2-dimensional laminar solution of the HVBK equations which can be derived

by applying Geurst's approach [5] for a cylindrical pipe to Cartesian geometry [15]. Indeed, Fig. 2 (right) shows that case (b) and this laminar solution [15] are very similar (with the exception of the channel axis, where Guerst's solution is singular and $n^* \to \infty$).

In Fig. 2 (left) we compare the analytical solution corresponding to nucleation at the walls ($\xi = 0$) to the velocity profile $\bar{v}_s^*(y^*)$ for case (c). It is apparent that, with decreasing ξ, $\bar{v}_s^*(y^*)$ tends to the analytical solution (the difference which is present near the walls arises from the boundary conditions for the superfluid velocity which ensure infinite vorticity in the nucleation region [5, 15]).

Further work will generalise the approach which we have presented, by solving self-consistently the equation for the normal fluid in the presence of the mutual friction, rather than assuming a given profile for $\mathbf{v}_n$. We also plan to investigate the dependence of the profiles on the vortex densities. The current rapid progress of visualization techniques, such as the recently developed laser-induced fluorescence of metastable molecules [16], will clearly stimulate more work on the nature of laminar and turbulent profiles of helium II in channels.

Acknowledgements M.S. acknowledges a travel grant of the Istituto Nazionale di Alta Matematica. C.F.B.'s work is supported by the Leverhulme Trust.

References

1. G.P. Bewley, D.P. Lathrop, K.R. Sreenivasan, Nature **441**, 588 (2006)
2. T. Zhang, S.W. Van Sciver, Nat. Phys. **1**, 36 (2005)
3. J.T. Tough, in *Progress of Low Temperature Physics*, vol. VIII, ed. by D.F. Brewer (1982), p. 133. Chap. 3
4. D.J. Melotte, C.F. Barenghi, Phys. Rev. Lett. **80**, 4181 (1998)
5. J.A. Geurst, Phys. Lett. A **71**, 78 (1979)
6. L. Greengard, SIAM J. Sci. Stat. Comput. **11**, 603 (1990)
7. K.W. Schwarz, Phys. Rev. B **38**, 2398 (1988)
8. C.F. Barenghi, R.J. Donnelly, W.F. Vinen, J. Low Temp. Phys. **52**, 189 (1983)
9. J. Koplik, H. Levine, Phys. Rev. Lett. **71**, 1375 (1993)
10. R.N. Hills, P.H. Roberts, Arch. Ration. Mech. Anal. **66**, 43 (1977)
11. D.R. Ladner, J.T. Tough, Phys. Rev. B **20**, 2690 (1979)
12. K.P. Martin, J.T. Tough, Phys. Rev. B **27**, 2788 (1983)
13. R.J. Donnelly, C.F. Barenghi, J. Phys. Chem. Ref. Data **27**, 1217 (1998)
14. C.F. Barenghi, S. Hulton, D.C. Samuels, Phys. Rev. Lett. **89**, 275301 (2002)
15. L. Galantucci, C.F. Barenghi, M. Sciacca, in preparation
16. W. Guo, S.B. Cahn, J.A. Nikkel, W.F. Vinen, D.N. McKinsey, arXiv:1004.2545 (2010)